

Porocoustoelasticity for rocks with a dual-pore structure

Wenchang Ling¹, Jing Ba¹, José M. Carcione², and Lin Zhang¹

ABSTRACT

Acoustoelasticity describes the interaction of acoustic waves with nonlinear elastic deformations, particularly the change of wave velocity due to initial stresses or strains in a predeformed body. The theory extends the strain energy to cubic terms (third-order elasticity) and allows for finite strains to model deformations at high confining pressures. However, the theory considers equant (stiff) pores but neglects the effects of soft (compliant) pores, such as microfractures, cracks, and grain contacts. Our main contribution is to include these effects. Application of the novel porocoustoelasticity theory to ultrasonic measurements on carbonate samples at varying confining pressures provides a better fit for the measured data of pressure dependence of wave velocity. We have quantified the contribution of the compliant pores to the nonlinear behavior of the wave velocity and determined the relation between the threshold pressure (beyond which the theories with and without compliant pores yield the same velocity) and porosity and permeability. The extension of porocoustoelasticity theory by incorporating a dual-pore structure provides better description for stress dependence of wave velocity in fluid-saturated heterogeneous rocks, which can be applicable in further field studies regarding reservoir characterization and in situ stress estimation.

INTRODUCTION

In situ tectonic stress variations play an important role in reservoir rock properties, including seismic wave velocities. The pressure dependence of the velocity variations includes linear and nonlinear behavior that cannot be described by the linear theory of elasticity.

Theoretical models of nonlinear elasticity are proposed by [Guyer and Johnson \(1999, 2009\)](#) and by [Guyer et al. \(1995\)](#) to simulate wave propagation using the Preisach-Mayergoyz space ([Mayergoyz, 1985](#)). [Lyakhovsky et al. \(1997\)](#) propose a damage rheology model without using finite strains, and [Vakhnenko et al. \(2006\)](#) introduce the soft ratchet model for longitudinal vibrations in sedimentary rocks. Recently, [Sens-Schönfelder et al. \(2019\)](#) propose a model for nonlinear elasticity in rocks, based on friction of internal interfaces and the process of contact aging. These theories incorporate the influence of cracks, but neglect the nonlinear acoustoelasticity and fluid deformation. [Mavko et al. \(1995\)](#) develop a simple method to predict stress-induced anisotropy in dry Barre Granite and Massillon Sandstone, where the approach does not assume a specific crack geometry and is not limited to small crack densities. However, this model considers the influence of cracks from a macroscopic perspective and is not suitable to study the pressure dependence of crack porosity, aspect ratio, and density.

To explain the nonlinear behaviors of materials, the concepts of hyperelasticity and acoustoelasticity have been developed, which involve third-order elastic constants (3oEC) ([Murnaghan, 1937](#); [Hughes and Kelly, 1953](#); [Thurston and Brugger, 1964](#); [Johnson, 1981](#); [Johnson, 1983](#); [Pao and Gamer, 1985](#); [Shams et al., 2011](#)). These nonlinear elasticity theories have been applied to rock mechanics ([Johnson and Shankland, 1989](#); [Meegan et al., 1993](#)). [Winkler and Liu \(1996\)](#) successfully measure the 3oEC of dry rock samples and apply the acoustoelasticity theory, resulting in accurate predictions of stress-induced velocity variations. However, [Winkler and McGowan \(2004\)](#) perform similar experiments on water-saturated rocks and find that the results could not be well explained by the acoustoelasticity theory. A possible explanation is that the theory neglects the presence of the pore fluid.

Based on the linear theory of elasticity, [Biot \(1956a, 1956b\)](#) derives wave equations for a two-phase porous rock, where the coupling between the solid and fluid is taken into account. [Biot \(1973\)](#) develops a semilinear theory by using seven elastic constants for porous media, of which four characterize the linear behavior and

Manuscript received by the Editor 11 May 2020; revised manuscript received 20 September 2020; published ahead of production 11 October 2020; published online 07 January 2021.

¹Hohai University, School of Earth Sciences and Engineering, Nanjing 211100, China. E-mail: ccling_geo@outlook.com; jba@hhu.edu.cn (corresponding author); zlin@hhu.edu.cn.

²Hohai University, School of Earth Sciences and Engineering, Nanjing 211100, China and Istituto Nazionale di Oceanografia e di Geofisica Sperimentale (OGS), Borgo Grotta Gigante 42c, Sgonico, Trieste 34010, Italy. E-mail: jose.carcione@gmail.com.

© 2021 Society of Exploration Geophysicists. All rights reserved.

three the nonlinear behavior. The poroacoustoelasticity theory incorporates nonlinear terms into Biot's equations (Biot, 1956a, 1956b; Grinfeld and Norris, 1996; Donskoy et al., 1997; Guo et al., 2009; Ba et al., 2013), but the predicted velocities do not agree with the measurements at high pore pressures (Guo et al., 2009; Ba et al., 2013), where the velocity shows an exponential behavior as a function of differential pressure, possibly explained by the closure of microcracks.

The factors affecting wave velocity include mineralogical composition, porosity, pore fluid, and, particularly, pore structure (Tuncu et al., 1994; Agersborg et al., 2008; David and Zimmerman, 2012; Ba et al., 2017). Walsh (1965) describes rocks with a double-porosity system consisting of stiff and compliant pores, the latter represented by cracks, microfractures, and grain contacts. Walsh's model was established with the dual-pore structure, and he finds that compliant pores have a stronger influence on the dry-rock elastic moduli than stiff pores, and he develops a relation between these moduli and confining pressure P_c (pore pressure $P_f = 0$), which can be used to estimate the compliant porosity. Cheng and Toksöz (1979) use the effective modulus obtained by Kuster and Toksöz (1974) to estimate the porosity in sandstones, but their result showed that this theory is not suitable when the crack density is high. Other works have also considered this problem (Fortin et al., 2007; Tran et al., 2008; Izumotani and Onozuka, 2013).

Based on an exponential relation between crack density and pressure, Zimmerman et al. (1986) establish a method to estimate the compressibility of sandstones and obtain a distribution of compliant pores with different aspect ratios. Using the Mori-Tanaka theory (Mori and Tanaka, 1973), David and Zimmerman (2012) extend the Zimmerman model (D-Z model) to compute the porosity and the elastic moduli from dry-rock wave velocities. Duan et al. (2018) and Zhang et al. (2019) adopt this model to estimate the pore microstructure.

Here, we use the poroacoustoelasticity theory developed by Ba et al. (2013). Because this theory properly describes the deformation of stiff pores, we obtain the 3oEC from the velocities at high effective (differential) pressures. However, it neglects the influence of compliant pores. Fu and Fu (2018) use a dual-porosity model suggested by Shapiro (2003) to model the effect of nonlinear deformations due to compliant porosity by using a semiempirical equation, but due to the adjustable parameter in this model, it is difficult to perform quantitative analysis about compliant porosity. On the other hand, the D-Z model appears to be appropriate to estimate the variations in dry-rock elastic moduli and porosity caused by compliant pores. Hence, we extend the poroacoustoelasticity theory by incorporating this model and apply it to carbonate samples to illustrate its effectiveness.

ROCK-PHYSICS MODELS

The D-Z model

David and Zimmerman (2012) consider randomly oriented stiff and compliant pores, and they evaluate the elastic properties of the rock skeleton in three steps (Walsh, 1965).

Step 1: Walsh (1965) provides the following expression for the effective bulk compliance of the dry rock:

$$C_{\text{eff}} = C_0 - \frac{d\phi}{dP}, \quad (1)$$

where $C_0 = 1/K_{\text{gr}}$ is the bulk compliance of the grains, with K_{gr} as the bulk modulus of the grains, and ϕ is the total porosity. Note that C_{eff} is related to the rate of change of porosity with pressure rather than porosity directly.

Step 2: Stiff pores are added into the rock matrix to create the host material. According to the Mori-Tanaka theory (Mori and Tanaka, 1973), the effective bulk and shear compliances of the rock containing only stiff pores are, respectively,

$$\begin{aligned} C_{\text{stiff}} &= C_0 \left(1 + \frac{\phi_{\text{stiff}}}{1-\phi_{\text{stiff}}} P^* \right) \\ S_{\text{stiff}} &= S_0 \left(1 + \frac{\phi_{\text{stiff}}}{1-\phi_{\text{stiff}}} Q^* \right), \end{aligned} \quad (2)$$

where $K_{\text{stiff}} = 1/C_{\text{stiff}}$ and $G_{\text{stiff}} = 1/S_{\text{stiff}}$ are the respective moduli. The shear compliance of the grains is $S_0 = 1/G_{\text{gr}}$, where G_{gr} is the shear modulus, ϕ_{stiff} is the stiff porosity, and P^* and Q^* are geometric factors (Wu, 1966).

Step 3: Compliant pores are added into the host material to complete the model. Different effective-medium theories may give dissimilar crack densities. David and Zimmerman (2012) compare the Mori-Tanaka and differential effective-medium schemes, but there is a small difference between the results of the two theories, with the first theory better describing the exponential pressure dependence of the bulk compressibility, which is consistent with the empirical law by Zimmerman et al. (1986) (it was established based on observations in sandstones). By neglecting the interactions between stiff and compliant pores, the effective bulk and shear compliances C_{eff} and S_{eff} are (David and Zimmerman, 2012), respectively,

$$\begin{aligned} C_{\text{eff}} &= C_{\text{stiff}} \left(1 + \frac{16(1 - (v_{\text{stiff}})^2)\Gamma}{9(1 - 2v_{\text{stiff}})} \right) \\ S_{\text{eff}} &= S_{\text{stiff}} \left(1 + \frac{32(1 - v_{\text{stiff}})(5 - v_{\text{stiff}})\Gamma}{45(2 - v_{\text{stiff}})} \right), \end{aligned} \quad (3)$$

where $v_{\text{stiff}} = (3K_{\text{stiff}} - 2G_{\text{stiff}})/(6K_{\text{stiff}} + 2G_{\text{stiff}})$; Γ is the crack density; and $K_{\text{eff}} = 1/C_{\text{eff}}$ and $G_{\text{eff}} = 1/S_{\text{eff}}$ are the respective moduli.

The crack porosity ϕ_c is obtained via the crack density Γ and the aspect ratio α as

$$\phi_c = \frac{4}{3}\pi\alpha\Gamma. \quad (4)$$

The relation between the crack density and the differential pressure P (MPa) is empirical and has the form

$$\Gamma(P) = \Gamma_0 e^{-P/\hat{p}}, \quad (5)$$

where \hat{p} is a compaction coefficient.

The relationship between a crack with initial aspect ratio α_i and the closure pressure P_{close} is (Walsh, 1965)

$$\alpha_i = \frac{4(1 - v_{\text{stiff}}^2)P_{\text{close}}}{\pi E_{\text{stiff}}}, \quad (6)$$

where $E_{\text{stiff}} = 3K_{\text{stiff}}(1 - 2v_{\text{stiff}})$ is the Young's modulus of the host material.

David and Zimmerman (2012) study the relationship between the aspect ratio distribution and the compliant porosity, whereas in the

present work we analyze the pressure dependence of the compliant porosity based on equation 6. This porosity decreases due to the closure of cracks with initial aspect ratio α_i , and the decrement is given from equation 4,

$$d\phi_c = \frac{4}{3}\pi\alpha_i d\Gamma. \quad (7)$$

Substituting equations 5 and 6 into equation 7, we obtain

$$d\phi_c = -\frac{16(1-v_{\text{stiff}}^2)P}{3\pi E_{\text{stiff}}\hat{p}}\Gamma_0 e^{-P/\hat{p}} dP. \quad (8)$$

By integration of equation 8, we obtain the porosity decrement of compliant pores for all pressures. Because the deformation of stiff pores is smaller than compliant pores, the variation in the porosity of stiff pores can be neglected. Then, the total porosity is

$$\phi = \phi_0 + d\phi_c, \quad (9)$$

where ϕ_0 is the initial porosity.

Poroacoustoelasticity

Poroacoustoelasticity extends the strain energy function to cubic terms and adopts the finite strain theory, because the infinitesimal strain theory is inappropriate to describe deformations at high confining pressures. The Lagrangian strain tensors are

$$\begin{cases} A_{ij} = \frac{1}{2}(u_{j,i} + u_{i,j} + u_{k,i}u_{k,j}), & i, j, k = 1, 2, 3 \\ B_{i(i)} = U_{(i),i} + \frac{1}{2}U_{(i),i}^2 \end{cases}, \quad (10)$$

where u_i and U_i denote the solid and fluid displacements, respectively, in the x_i -direction, and A and B are the solid and fluid strains, respectively.

The solid and fluid stress components σ_{ij} and τ_{ij} are obtained from the strain energy function W ,

$$\sigma_{ij} = \frac{\partial W}{\partial A_{ij}} \quad \text{and} \quad \tau_{ij} = \frac{\partial W}{\partial B_{ij}}, \quad i, j = 1, 2, 3. \quad (11)$$

Based on the low-frequency limit of Biot's equations (Biot, 1956a), by neglecting the interaction between the solid and fluid phases, the resulting velocity expressions of the poroacoustoelasticity theory, under hydrostatic stress conditions, are (Ba et al., 2013)

$$\begin{cases} \rho V_p^2 = (K_{\text{dr}} + Mn^2 + \frac{4}{3}G_{\text{dr}}) + \Psi_1 A + \Psi_2 B \\ \rho V_s^2 = G_{\text{dr}} + \Psi_3 A + \Psi_4 B \end{cases}, \quad (12)$$

where V_p and V_s are the compressional wave (P-wave) and shear-wave (S-wave) velocities, respectively; K_{dr} and G_{dr} are the dry-rock bulk and shear moduli, respectively; ρ is the saturated-rock density; the coupling modulus of fluid-saturated rock M and the Biot's coefficient n are

$$\begin{cases} n = 1 - \frac{K_{\text{dr}}}{K_{\text{gr}}} \\ M = \frac{K_{\text{gr}}}{1 - \phi \frac{K_{\text{dr}}}{K_{\text{gr}}} + \phi \left(\frac{K_{\text{gr}}}{K_{\text{f}}}\right)}, \end{cases} \quad (13)$$

where K_{f} is the bulk modulus of the pore fluid.

In linear elasticity, the potential energy is a quadratic function of strain, whereas here (the poroacoustoelasticity theory) it is a cubic function of strain (the coefficients in the n -order terms are termed the n -order elastic constants). Equation 12 gives the synthetic elastic constants Ψ_j ($j = 1, 2, 3, 4$) containing the 3oEC,

$$\begin{cases} \Psi_1 = 7M_1 + M_2 + \frac{7}{2}M_4 + 9M_5 + 2M_8 + M_9 + 3M_{10} + 3M_{11} \\ \Psi_2 = 7M_3 + \frac{7}{2}M_4 + 9M_7 + 3M_{10} + 3M_{11} \\ \Psi_3 = 3M_1 - \frac{1}{4}M_6 - \frac{3}{4}M_8 \\ \Psi_4 = \frac{3}{2}M_4 - \frac{3}{4}M_9 \end{cases}, \quad (14)$$

where M_i ($i = 1, 2, 3, 4$) and M_j ($j = 5, 6, n, 11$) are the second-order elastic constants and 3oEC, respectively. A comprehensive review can be found in Ba et al. (2013). The positive elastic strains A and B of the rock matrix and pore fluid in stiff pores, respectively, are (see Appendix A)

$$\begin{cases} A = \frac{P_c - \phi P_f}{3(1-\phi)K_{\text{gr}}} \\ B = \frac{\theta - (1-\phi)3A}{3\phi} \end{cases}, \quad (15)$$

where P_c and P_f are the confining and pore pressures, respectively, and

$$\theta = \frac{P_c - nP_f}{K_{\text{dr}}} \quad (16)$$

is the bulk strain.

At high confining pressures, compliant pores tend to close, and the poro-acoustoelasticity theory can be used to calculate the 3oEC related to the stiff pores (Fu and Fu, 2018). The figure in Appendix B describes the rock-physics model.

EXPERIMENTAL DATA

We compare experimental data, obtained in the laboratory for carbonates, with the theory with and without compliant pores. The five carbonate samples (E1, E2, E3, F1, and F2) have been collected from the Cambrian formations of the Tarim Basin, Northwest China, and the other three samples (A, B, C) have been collected from the Permian formations, Sichuan Basin, Southwest China. The samples are granular dolomites with dissolved pores, whose properties are given in Table 1. The in situ confining pressure and temperature of the two formations are approximately 80 MPa and 140°C, respectively, whereas the depth exceeds 4 km. The experimental setup is that of Guo et al. (2009). The samples were saturated with oil (kerosene) at confining pressures increasing from 20 to 80 MPa, at a constant pore pressure of 10 MPa, and a temperature of 140°C. Measurements were also performed at full gas (nitrogen) and water saturations at 80 MPa and 140°C. We measured P- and S-wave velocities using piezoelectric transducers at a range of confining pressures and amplitude of the signal. Figure 1 shows how the confining pressure affects amplitude of the signal, which is representative of all samples.

MODELING

Estimations of the dry-rock moduli and total porosity

The saturated-rock bulk and shear moduli K_w and G_w are obtained from the measured velocities,

$$K_w = \rho((V_P)^2 - \frac{4}{3}(V_S)^2), \quad G_w = \rho(V_S)^2. \quad (17)$$

Then, the dry-rock elastic moduli K_{dr} and G_{dr} are obtained from the high-frequency ones of [Mavko and Jizba \(1991\)](#).

The D-Z model requires the following four steps.

Step 1: Evaluate the crack density at each pressure. Because compliant pores tend to close at high differential pressure (in this range, we assume that the most compliant pores are closed and categorize those remaining as stiff pores, which can be well described by acoustoelasticity), we use the dry-rock elastic moduli in this range ($K_{stiff} \approx K_{dr}^{hp}$ and $G_{stiff} \approx G_{dr}^{hp}$) to obtain the crack density. Based on the moduli calculated from equation 17, we use equation 3 ($K_{eff} = K_{dr}$ and $G_{eff} = G_{dr}$) to obtain the crack density Γ by a least-squares regression at the differential pressure P .

Step 2: Obtain the fitting parameters of Γ_0 and \hat{p} based on P and Γ . To obtain the crack density at all pressures, we use equation 5 to fit the discrete data points obtained in step 1.

Step 3: Establish the relation between K_{dr} , G_{dr} , and P . To obtain the pressure dependence of the effective moduli (the dry-rock elastic moduli), we substitute equation 5 into equation 3 to calculate the moduli for all of the differential pressures.

Step 4: Establish the relation between P and ϕ . By using the fitting parameters calculated from step 2, the relation between the total porosity and differential pressure is obtained by combining equations 8 and 9.

Estimations of the 3oEC

To estimate the synthetic elastic constants $\Psi_j (j = 1, 2, 3, 4)$ accurately, we use two sets of velocity measurements of the P- and S-waves at high confining pressures P_c^{h1} and P_c^{h2} . First, we calculate the elastic strains A and B of the rock matrix and pore fluid in the stiff pores from equation 15,

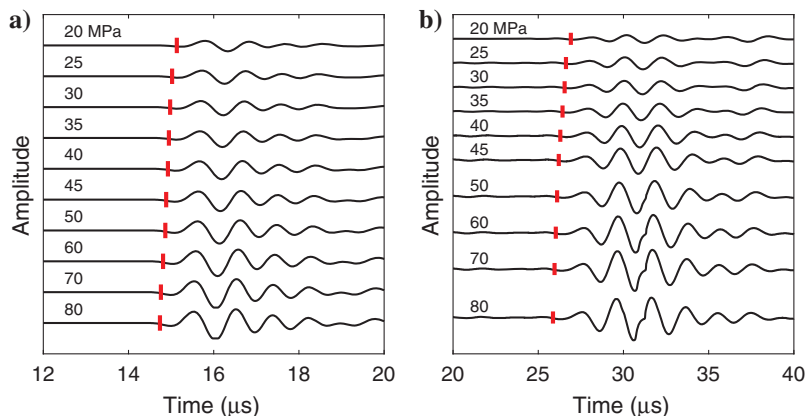


Figure 1. (a) P and (b) S waveforms at different confining pressures for sample A. Red marks are the picks at which the traveltimes is taken.

Table 1. Properties of the carbonate samples.

Lithology	Dry-rock density (g/cm ³)	Porosity (%)	Permeability (mD)	
A	2.45	11.63	0.661	
B	2.51	11.73	0.138	
C	2.45	11.75	0.075	
Dolomite	E1	2.69	5.10	
	E2	2.66	5.34	
	E3	2.67	5.47	
	F1	2.41	12.08	162.753
	F2	2.44	12.28	22.819

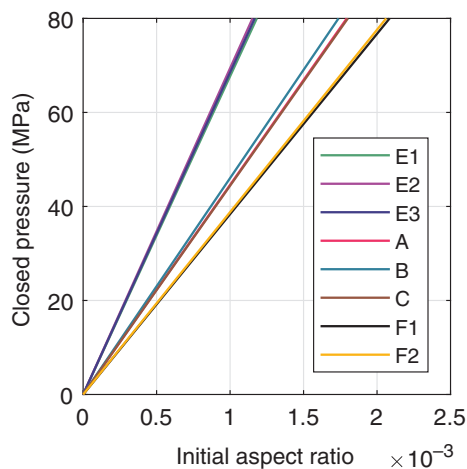


Figure 2. Pore-closed pressure as a function of initial aspect ratio of closed pores for all samples. The legend indicates the sample number.

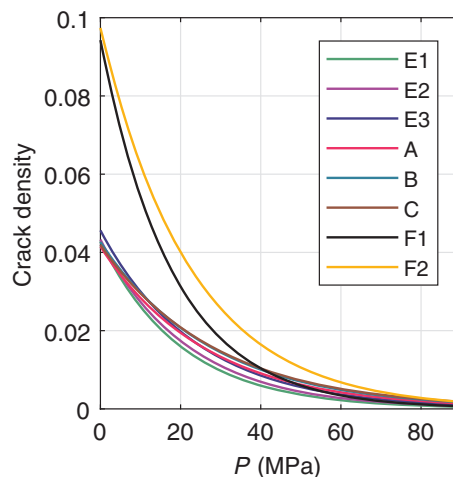


Figure 3. Crack density as a function of differential pressure for all samples. Crack density decreases with differential pressure and approaches zero at the high pressures. The compliant pores tend to close with the increasing differential pressure. The legend indicates the sample number.

$$\begin{cases} A|_{P_c=P_c^{h1}} = \frac{P_c - \phi P_f}{3(1-\phi)K_{gr}} \\ B|_{P_c=P_c^{h1}} = \frac{\theta - 3(1-\phi)B}{3\phi} \end{cases} \quad (18)$$

and

$$\begin{cases} A|_{P_c=P_c^{h2}} = \frac{P_c - \phi P_f}{3(1-\phi)K_{gr}} \\ B|_{P_c=P_c^{h2}} = \frac{\theta - 3(1-\phi)A}{3\phi} \end{cases} \quad (19)$$

The density of the pore fluid at the experimental conditions is obtained with the empirical equations of [Batzle and Wang \(1992\)](#). By combining the dry-rock density and the porosity, the fluid density estimated above provides the density of the saturated rock ρ . By substituting the rock and fluid properties into equation 12, we combine equations 12, 18, and 19 to obtain the synthetic elastic constants $\Psi_j (j = 1, 2, 3, 4)$.

RESULTS

Elastic rock properties analysis based on the D-Z model

The compliant pores mainly dictate the rock properties at low pressures. According to equation 6, microcracks with the initial aspect ratio α_i close at the different pressure P_{close} . As shown in Figure 2, the pore-closed pressure P_{close} increases linearly with the initial aspect ratio of the compliant pores. The aspect ratios are generally less than 0.01 for all experimental pressures. This value is taken as the limit between stiff and compliant pores.

Figure 3 shows that the crack density of the eight samples decreases with pressure, as expected, because the compliant pores close for increasing differential pressures. Figure 4 displays the compliant-porosity decrement of the crack porosity as a function of pressure. The dry-rock moduli are shown in Figure 5 (based on equation 5), where the trend is similar to that of Figure 4. As the differential pressure increases, compliant pores close and this increases the stiffness of the rock. Figure 6 shows the dry-rock moduli as a function of the compliant-porosity decrement, illustrating the contribution of compliant pores to the nonlinear behavior of the rock properties.

Wave velocity based on the poroacoustoelasticity and D-Z models

In this case, the stiffness moduli, porosity, and 3oEC, $\Psi_j (j = 1, 2, 3, 4)$, are needed. The latter are estimated by substituting the measured velocities at high pressures in equation 12, whereas the dry-rock elastic moduli and porosity are estimated with the D-Z model. Figure 7 compares the velocities predicted by the poroacoustoelasticity theory with and without compliant pores. The agreement with the experimental data is good at high pressures, but the theory without compliant pores has a large deviation at low pressures. For the P waves, the poroacoustoelastic theory, combined with the D-Z model, agrees well with the measurements. The disagreement at low pressures may be due to pore connections, because these are neglected in the theory (compliant pores are assumed to be independent of each other).

Figure 8 compares theory and experiment, where oil has been replaced by gas and water. The data corresponds to a confining pressure of 80 MPa and a temperature of 140°C. As can be seen, the predictions agree with the experimental measurements. The discrepancy can be explained by the fact that we used experimental data at high pressures to compute the elastic constants of the host material, where all the cracks are assumed to be closed. Instead, some cracks may not be completely closed for the considered carbonate samples. To analyze the contribution of the compliant pores to the P-wave velocity, we define the differential pressure at which the theories with and without compliant pores yield approximately the same velocity within an error of 1%, called the threshold pressure. Let us denote this velocity yielded by the theory with (without) compliant pores by $V_p^{(T1)}$ ($V_p^{(T2)}$). We define $R = (V_p^{(T1)} - V_p^{(1)}) / (V_p^{(T2)} - V_p^{(2)})$, where $V_p^{(1)}$ and $V_p^{(2)}$ are the velocities of the theory without and with compliant pores, respectively, at differential pressures lower than the threshold pressure. Then, the contribution of compliant pores is $1 - R$. As shown in Figure 9, this value decreases

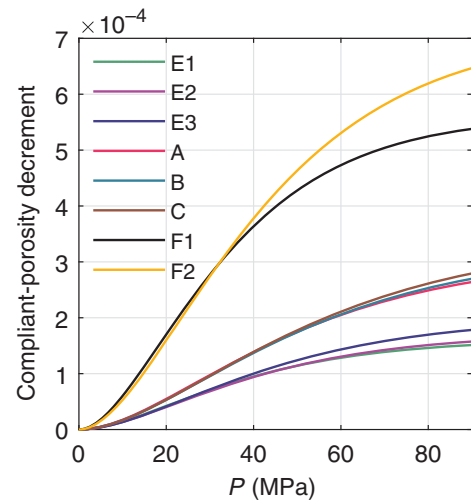


Figure 4. Compliant-porosity decrement as a function of differential pressure. The vertical axis is the absolute value of the cumulative compliant-porosity variation from 0 MPa to P . The legend indicates the sample number.

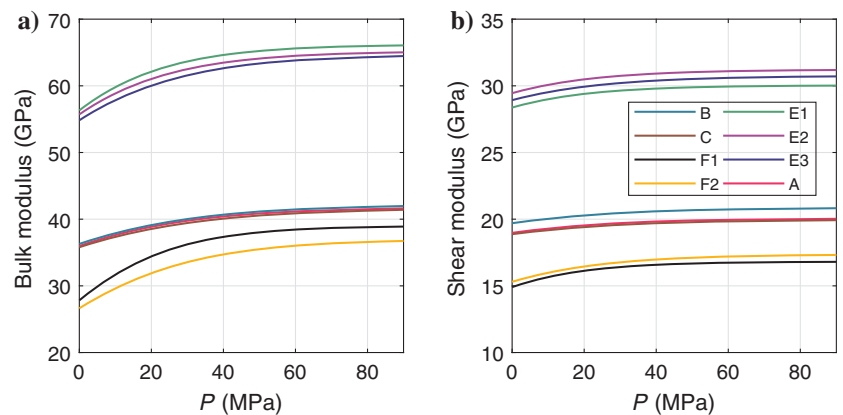


Figure 5. (a) Dry-rock bulk modulus and (b) shear modulus of the eight samples as a function of the differential pressure. The legend applies to both panels.

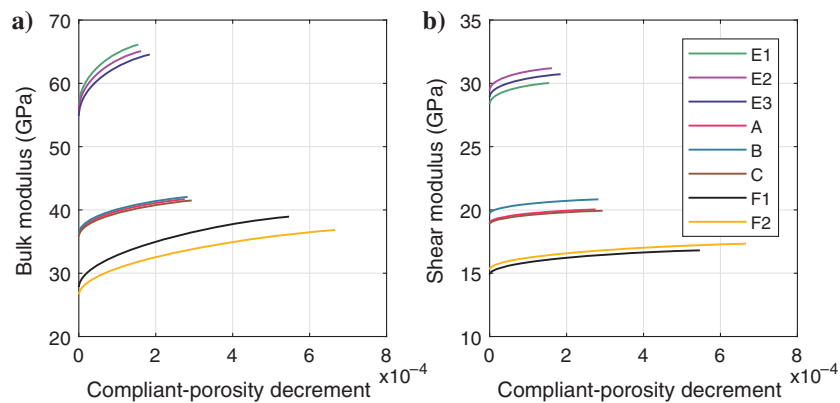


Figure 6. (a) Dry-rock bulk modulus and (b) shear modulus as a function of the compliant-porosity decrement. The horizontal axis is the absolute value of the cumulative compliant-porosity variation from 0 MPa to P , and the lines stop because the compliant pores tend to close. The legend applies to both panels.

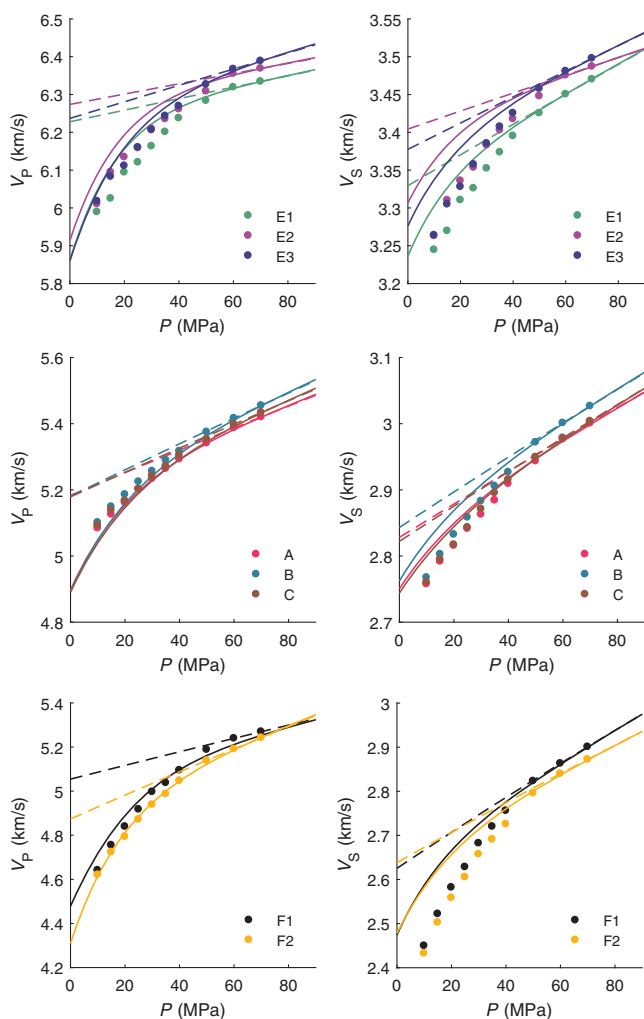


Figure 7. P- and S-wave velocities as a function of differential pressure. The full circles correspond to the measurements. The solid lines and dashed lines correspond to the poroacoustoelasticity theory with and without compliant pores, respectively. The agreement between the theory and the experiment is good except for low pressures for some samples. This discrepancy may come from connected pores, which are not included in the theory.

with differential pressure, indicating that the poroacoustoelasticity with compliant pores is more effective to describe stress-induced velocity at lower pressures. The higher threshold-pressure values of sample F1 (the black curve) can be attributed to significant pore connections, because this sample has high permeability given its porosity.

As shown in Figure 10, the threshold pressure increases with the initial porosity, but, as above, the differences can be due to the presence of connections between the compliant pores. The same pressure as a function of permeability is shown in Figure 11. It increases with permeability, i.e., possibly related to more pore connections.

DISCUSSION

Unlike many nonlinear elastic models, poroacoustoelasticity focuses on the stress dependence of velocity, including the solid and fluid strains, up to the 3oEC. In this work, we introduce the D-Z model to modify the theory by considering the influence of the compliant pores.

We analyze the two fitting parameters of the D-Z model based on the high-pressure approximation. Then, we model the pressure dependence of the crack properties, whereas the original theory describes the relation between the crack properties and the distribution of aspect ratios (David and Zimmerman, 2012; Duan et al. 2018; Zhang et al. 2019). Shapiro (2003) provides a simple model to study crack deformation, with a semiempirical model based on a Taylor expansion. Fu and Fu (2018) use Shapiro's model to obtain the nonlinear velocity predictions, which are similar to the results of this study (as shown in Figure 7); nevertheless, there is an adjustable

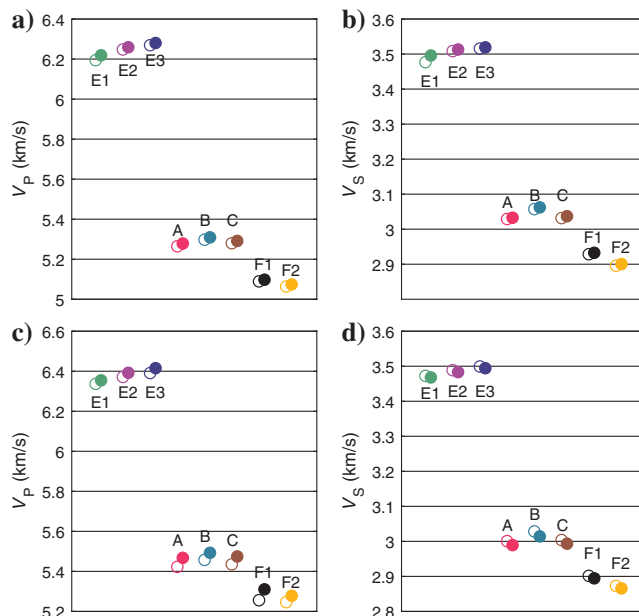


Figure 8. Wave velocities at a confining pressure of 80 MPa: (a) P-wave and (b) S-wave for full gas saturation; (c) P-wave and (d) S-wave for full water saturation. The solid and empty circles correspond to the experiment and the theory, respectively.

parameter ϕ_{cdrs} and an underdetermined initial porosity ϕ_{c0} in the Fu and Fu theory. In this work, a cumulative compliant-porosity decrement is introduced. Figure 4 shows this decrement as a function of differential pressure, which approaches a constant value at high differential pressures. By assuming that the compliant pores close at high pressures, the computed cumulative-compliant porosity decrement is approximately equal to the initial compliant porosity. In this manner, we avoid having to evaluate the initial compliant porosity ϕ_{c0} of Fu and Fu (2018).

The limitation of the poroacoustoelasticity theory is the measurement of the 3oEC (Biot, 1973; Norris et al., 1994; Degtyar and Rokhlin, 1998; Ba et al., 2013). Compliant porosity varies with stress, resulting in variations of the second-order elastic constants of the rock skeleton. Similarly, the 3oEC also depend on stress, due to variations of the compliant porosity; i.e., Ψ_j in equation 12 depends on pressure. Ba et al. (2013) and Fu and Fu (2018) neglect this effect, although their predictions fit experimental data.

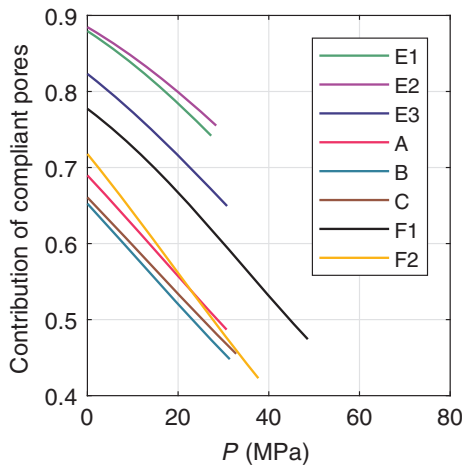


Figure 9. The distribution of the discrepancy between the two theories for P-wave velocity, reflecting the contribution of compliant pores to stress-induced velocities. The lines stop at the threshold pressures where the compliant pores tend to close (the influence of the remaining compliant pores can be neglected).

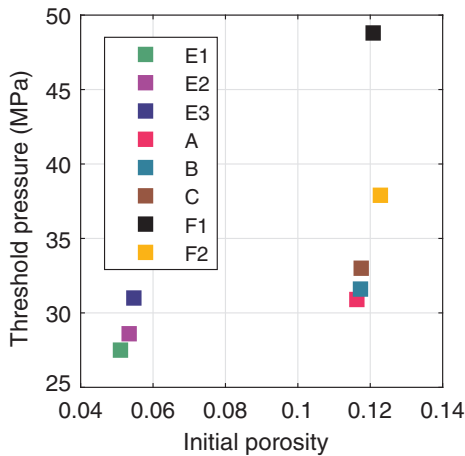


Figure 10. Differential pressure at which the theories with and without compliant pores yield the same result as a function of initial porosity for all samples.

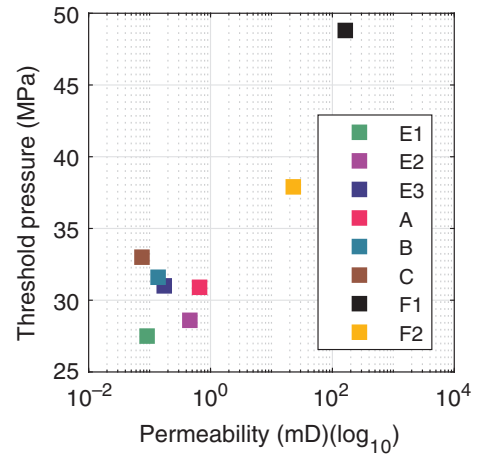


Figure 11. Differential pressure at which the theories with and without compliant pores yield the same result as a function of permeability for all samples.

However, the effect of compliant-pore variation on 3oEC is still unclear and must be considered in future work.

In this work, we introduce a threshold pressure to differentiate the applications of poroacoustoelasticity with and without compliant pores in carbonates. Figure 9 quantitatively shows that the theory with compliant pores is more effective for describing the wave velocity in the pressure range below the threshold pressure. Higher initial porosity may be associated with higher compliant porosity (Zhang and Bentley, 2003) and higher permeability indicates a higher degree of pore connection. Figures 10 and 11 show that a higher initial porosity and permeability could be related to higher threshold pressures in carbonates, i.e., a stronger impact of compliant pores on rock properties. Furthermore, wave-induced fluid flow, which is associated with compliant microcracks, may lead to wave anelasticity and attenuation (Guo et al., 2018a, 2018b), which is not considered in this study. To incorporate the effect of wave-induced fluid flow into the traditional acoustoelasticity theory will result in even more complicated mathematical equations, which may be considered in a future work.

CONCLUSION

Poroacoustoelasticity describes the nonlinear behavior of rocks caused by the deformation of stiff pores as a function of differential pressure. Generalizing this theory by including the effects of compliant pores (cracks, microfractures) improves the agreement between theory and experiment. The new theory is applied to model the wave velocities of carbonate samples as a function of differential pressure. The results lead to the following conclusions: (1) the novel theory considers the effects of stiff and compliant pores on the rock properties and matches the data at all differential pressures; (2) the original and novel poroacoustoelasticity theories predict the same velocities at high confining pressures, when all of the compliant pores tend to close; (3) the differential pressure threshold at which the two theories coincide increases with porosity and permeability; and (4) the creation of pore connections, neglected by the novel theory, can be the cause of mismatches with the experimental data.

DATA AND MATERIALS AVAILABILITY

Data associated with this research are available and can be obtained by contacting the corresponding author.

APPENDIX A

ELASTIC STRAINS IN POROELASTICITY THEORY

The elastic strains A and B of the rock matrix and pore fluid in stiff pores, respectively, are given in Gassmann (1951):

$$\begin{aligned}
 -\frac{\Delta V_s}{V} &= \frac{P_c - P_f}{K_{gr}} + (1 - \phi) \frac{P_f}{K_{gr}} = \frac{P_c - \phi P_f}{K_{gr}} \\
 -\frac{\Delta V_s}{V_s} &= -\frac{\Delta V_s}{V(1 - \phi)} = \frac{P_c - \phi P_f}{(1 - \phi)K_{gr}} \\
 A &= \frac{P_c - \phi P_f}{3(1 - \phi)K_{gr}} \\
 -\frac{\Delta V}{V} &= \frac{P_c - P_f}{K_{dr}} + \frac{P_f}{K_{gr}} = \theta \\
 -\frac{\Delta V}{V} &= -\frac{\Delta V_s + \Delta V_f}{V} = -\frac{\Delta V_s}{V} + \left(-\frac{\Delta V_f}{V}\right) \\
 -\frac{\Delta V_f}{V} &= -\frac{\Delta V}{V} - \left(-\frac{\Delta V_s}{V}\right) = \theta - \frac{P_c - \phi P_f}{K_{gr}} = \theta - 3(1 - \phi)A \\
 -\frac{\Delta V_f}{V_f} &= -\frac{\Delta V_f}{V\phi} = \frac{\theta - 3(1 - \phi)A}{\phi} \\
 B &= \frac{\theta - 3(1 - \phi)A}{3\phi}, \tag{A-1}
 \end{aligned}$$

where V_s , V_f , and V denote the solid volume, fluid volume, and total rock volume, respectively, and Δ denotes the differential value.

APPENDIX B

WORKFLOW OF ROCK-PHYSICS MODEL

The rock-physics model of the poroacoustoelasticity theory with a dual-pore structure is constructed by the workflow shown in Figure B-1.

REFERENCES

- Agersborg, R., T. A. Johansen, M. Jakobsen, J. Sothcott, and A. Best, 2008, Effects of fluids and dual-pore systems on pressure-dependent velocities and attenuations in carbonates: *Geophysics*, **73**, no. 5, N35–N47, doi: [10.1190/1.2969774](https://doi.org/10.1190/1.2969774).
- Ba, J., J. M. Carcione, H. Cao, F. Yao, and Q. Du, 2013, Poro-acoustoelasticity of fluid-saturated rocks: *Geophysical Prospecting*, **61**, 599–612, doi: [10.1111/j.1365-2478.2012.01091.x](https://doi.org/10.1111/j.1365-2478.2012.01091.x).
- Ba, J., W. Xu, L. Y. Fu, J. M. Carcione, and L. Zhang, 2017, Rock anelasticity due to patchy saturation and fabric heterogeneity: A double double-porosity model of wave propagation, *Journal of Geophysical Research: Solid Earth*, **122**, 1949–1976, doi: [10.1002/2016JB013882](https://doi.org/10.1002/2016JB013882).
- Batzle, M. L., and Z. Wang, 1992, Seismic properties of pore fluids: *Geophysics*, **57**, 1396–1408, doi: [10.1190/1.1443207](https://doi.org/10.1190/1.1443207).
- Biot, M. A., 1956a, Theory of propagation of elastic waves in a fluid-saturated porous solid. I: Low-frequency range: *The Journal of the Acoustical Society of America*, **28**, 168–178, doi: [10.1121/1.1908239](https://doi.org/10.1121/1.1908239).
- Biot, M. A., 1956b, Theory of propagation of elastic waves in a fluid-saturated porous solid. II: Higher frequency range: *The Journal of the Acoustical Society of America*, **28**, 179–191, doi: [10.1121/1.1908241](https://doi.org/10.1121/1.1908241).
- Biot, M. A., 1973, Nonlinear and semilinear rheology of porous solids: *Journal of Geophysical Research*, **78**, 4924–4937, doi: [10.1029/JB078i023p04924](https://doi.org/10.1029/JB078i023p04924).
- Cheng, C. H., and M. N. Toksöz, 1979, Inversion of seismic velocities for the pore aspect ratio spectrum of a rock: *Journal of Geophysical Research, Solid Earth*, **84**, 7533–7543, doi: [10.1029/JB084iB13p07533](https://doi.org/10.1029/JB084iB13p07533).
- David, E. C., and R. W. Zimmerman, 2012, Pore structure model for elastic wave velocities in fluid-saturated sandstones: *Journal of Geophysical Research, Solid Earth*, **117**, 185–201, doi: [10.1029/2012JB009195](https://doi.org/10.1029/2012JB009195).
- Degtyar, A. D., and S. I. Rokhlin, 1998, Stress effect on boundary conditions and elastic wave propagation through an interface between anisotropic media: *The Journal of the Acoustical Society of America*, **104**, 1992–2003, doi: [10.1121/1.423765](https://doi.org/10.1121/1.423765).
- Donskoy, D. M., K. Khashanah, and T. G. McKee Jr., 1997, Nonlinear acoustic waves in porous media in the context of Biot's theory: *The Journal of the Acoustical Society of America*, **102**, 2521–2528, doi: [10.1121/1.421011](https://doi.org/10.1121/1.421011).

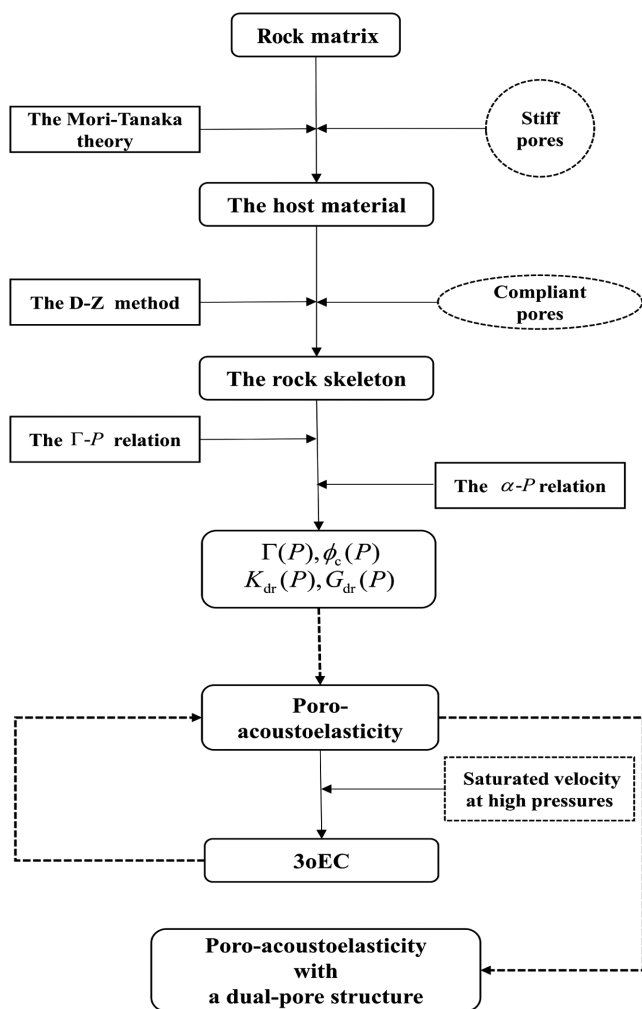


Figure B-1. Flowchart for rock-physics model. The effective elastic moduli of the rock skeleton are obtained by using the Mori-Tanaka theory and the D-Z model to analyze the effects of stiff and compliant pores, respectively. Crack parameters including crack density, crack aspect ratio, and crack porosity are estimated based on the relations between crack parameters and differential pressure. The 3oEC is determined by using the velocities of saturated rock at high pressures, based on the poro-acoustoelasticity theory. The model of this study is constructed by incorporating the effects of compliant pores at low differential pressures into poroacoustoelasticity theory.

- Duan, C., J. Deng, Y. Li, Y. Lu, Z. Tang, and X. Wang, 2018, Effect of pore structure on the dispersion and attenuation of fluid-saturated tight sandstone: *Journal of Geophysics and Engineering*, **15**, 449–460, doi: [10.1088/1742-2140/aa8b82](https://doi.org/10.1088/1742-2140/aa8b82).
- Fortin, J., Y. Guéguen, and A. Schubnel, 2007, Effects of pore collapse and grain crushing on ultrasonic velocities and Vp/Vs: *Journal of Geophysical Research, Solid Earth*, **112**, B08207, doi: [10.1029/2005JB004005](https://doi.org/10.1029/2005JB004005).
- Fu, B. Y., and L. Y. Fu, 2018, Poro-acoustoelasticity with compliant pores for fluid-saturated rocks: *Geophysics*, **83**, no. 3, WC1–WC14, doi: [10.1190/geo2017-0423.1](https://doi.org/10.1190/geo2017-0423.1).
- Gassmann, F., 1951, Elasticity of porous media: *Vierteljahrsschrder Naturforschenden Gessellschaft*, **96**, 1–23.
- Grinfeld, M. A., and A. N. Norris, 1996, Acoustoelasticity theory and applications for fluid-saturated porous media: *The Journal of the Acoustical Society of America*, **100**, 1368–1374, doi: [10.1121/1.415983](https://doi.org/10.1121/1.415983).
- Guo, J., J. Germán Rubino, N. D. Barbosa, S. Glubokovskikh, and B. Gurevich, 2018a, Seismic dispersion and attenuation in saturated porous rocks with aligned fractures of finite thickness: Theory and numerical simulations—Part 1: P-wave perpendicular to the fracture plane: *Geophysics*, **83**, no. 1, WA49–WA62, doi: [10.1190/geo2017-0065.1](https://doi.org/10.1190/geo2017-0065.1).
- Guo, J., J. Germán Rubino, N. D. Barbosa, S. Glubokovskikh, and B. Gurevich, 2018b, Seismic dispersion and attenuation in saturated porous rocks with aligned fractures of finite thickness: Theory and numerical simulations—Part 2: Frequency-dependent anisotropy: *Geophysics*, **83**, no. 1, WA63–WA71, doi: [10.1190/geo2017-0066.1](https://doi.org/10.1190/geo2017-0066.1).
- Guo, M., L. Fu, and B. Jing, 2009, Comparison of stress-associated coda attenuation and intrinsic attenuation from ultrasonic measurements: *Geophysical Journal International*, **178**, 447–456, doi: [10.1111/j.1365-246X.2009.04159.x](https://doi.org/10.1111/j.1365-246X.2009.04159.x).
- Guyer, R. A., and P. A. Johnson, 1999, Nonlinear mesoscopic elasticity: Evidence for a new class of materials: *Physics Today*, **52**, 30–36, doi: [10.1063/1.882648](https://doi.org/10.1063/1.882648).
- Guyer, R. A., and P. A. Johnson, 2009, Nonlinear mesoscopic elasticity: The complex behaviour of rocks, soil, concrete: John Wiley & Sons.
- Guyer, R. A., K. R. McCall, and G. N. Boitnott, 1995, Hysteresis, discrete memory, and nonlinear wave propagation in rock: A new paradigm: *Physical Review Letters*, **74**, 3491, doi: [10.1103/PhysRevLett.74.3491](https://doi.org/10.1103/PhysRevLett.74.3491).
- Hughes, D. S., and J. L. Kelly, 1953, Second-order elastic deformation of solids: *Physical Review*, **92**, 1145–1149, doi: [10.1103/PhysRev.92.1145](https://doi.org/10.1103/PhysRev.92.1145).
- Izumotani, S., and S. Onozuka, 2013, Elastic moduli and the aspect ratio spectrum of rock using simulated annealing: *Geophysical Prospecting*, **61**, 489–504, doi: [10.1111/1365-2478.12003](https://doi.org/10.1111/1365-2478.12003).
- Johnson, G. C., 1981, Acoustoelastic theory for elastic–plastic materials: *The Journal of the Acoustical Society of America*, **70**, 591–595, doi: [10.1121/1.386748](https://doi.org/10.1121/1.386748).
- Johnson, G. C., 1983, The effect of plastic deformation on the acoustoelastic response of metals: *Journal of Applied Mechanics*, **50**, 689–691, doi: [10.1115/1.3167116](https://doi.org/10.1115/1.3167116).
- Johnson, P. A., and T. J. Shankland, 1989, Nonlinear generation of elastic waves in granite and sandstone: Continuous wave and travel time observations: *Journal of Geophysical Research*, **94**, 17729–17733, doi: [10.1029/JB094iB12p17729](https://doi.org/10.1029/JB094iB12p17729).
- Kuster, G. T., and M. N. Toksöz, 1974, Velocity and attenuation of seismic waves in two-phase media: Part I. Theoretical formulations: *Geophysics*, **39**, 587–606, doi: [10.1190/1.1440450](https://doi.org/10.1190/1.1440450).
- Lyakhovskiy, V., Y. Ben-Zion, and A. Agnon, 1997, Distributed damage, faulting, and friction: *Journal of Geophysical Research, Solid Earth*, **102**, 27635–27649, doi: [10.1029/97JB01896](https://doi.org/10.1029/97JB01896).
- Mavko, G., and D. Jizba, 1991, Estimating grain-scale fluid effects on velocity dispersion in rocks: *Geophysics*, **56**, 1940–1949, doi: [10.1190/1.1443005](https://doi.org/10.1190/1.1443005).
- Mavko, G., T. Mukerji, and N. Godfrey, 1995, Predicting stress-induced velocity anisotropy in rocks: *Geophysics*, **60**, 1081–1087, doi: [10.1190/1.1443836](https://doi.org/10.1190/1.1443836).
- Mayergoyz, I. D., 1985, Hysteresis models from the mathematical and control theory points of view: *Journal of Applied Physics*, **57**, 3803–3805, doi: [10.1063/1.334925](https://doi.org/10.1063/1.334925).
- Meegan, G. D., Jr, P. A. Johnson, R. A. Guyer, and K. R. McCall, 1993, Observations of nonlinear elastic wave behavior in sandstone: *The Journal of the Acoustical Society of America*, **94**, 3387–3391, doi: [10.1121/1.407191](https://doi.org/10.1121/1.407191).
- Mori, T., and K. Tanaka, 1973, Average stress in matrix and average elastic energy of materials with misfitting inclusions: *Acta Metallurgica*, **21**, 571–574, doi: [10.1016/0001-6160\(73\)90064-3](https://doi.org/10.1016/0001-6160(73)90064-3).
- Murnaghan, F. D., 1937, Finite deformations of an elastic solid: *American Journal of Mathematics*, **59**, 235–260, doi: [10.2307/2371405](https://doi.org/10.2307/2371405).
- Norris, A. N., B. K. Sinha, and S. Kostek, 1994, Acoustoelasticity of solid/fluid composite systems: *Geophysical Journal International*, **118**, 439–446, doi: [10.1111/j.1365-246X.1994.tb03975.x](https://doi.org/10.1111/j.1365-246X.1994.tb03975.x).
- Pao, Y. H., and U. Gamer, 1985, Acoustoelastic waves in orthotropic media: *The Journal of the Acoustical Society of America*, **77**, 806–812, doi: [10.1121/1.392384](https://doi.org/10.1121/1.392384).
- Sens-Schönfelder, C., R. Snieder, and X. Li, 2019, A model for nonlinear elasticity in rocks based on friction of internal interfaces and contact aging: *Geophysical Journal International*, **216**, 319–331, doi: [10.1093/gji/ggy414](https://doi.org/10.1093/gji/ggy414).
- Shams, M., M. Destrade, and R. W. Ogden, 2011, Initial stresses in elastic solids: Constitutive laws and acoustoelasticity: *Wave Motion*, **48**, 552–567, doi: [10.1016/j.wavemoti.2011.04.004](https://doi.org/10.1016/j.wavemoti.2011.04.004).
- Shapiro, S. A., 2003, Elastic piezosensitivity of porous and fractured rocks: *Geophysics*, **68**, 482–486, doi: [10.1190/1.1567215](https://doi.org/10.1190/1.1567215).
- Thurston, R. N., and K. Brugger, 1964, Third-order elastic constants and the velocity of small amplitude elastic waves in homogeneously stressed media: *Physical Review*, **133**, A1604–A1610, doi: [10.1103/PhysRev.133.A1604](https://doi.org/10.1103/PhysRev.133.A1604).
- Tran, D. T., C. S. Rai, and C. H. Sondergeld, 2008, Changes in crack aspect-ratio concentration from heat treatment: A comparison between velocity inversion and experimental data: *Geophysics*, **73**, no. 4, E123–E132, doi: [10.1190/1.2928848](https://doi.org/10.1190/1.2928848).
- Tutuncu, A. N., A. L. Podio, and M. M. Sharma, 1994, An experimental investigation of factors influencing compressional-and shear-wave velocities and attenuations in tight gas sandstones: *Geophysics*, **59**, 77–86, doi: [10.1190/1.1443536](https://doi.org/10.1190/1.1443536).
- Vakhnenko, O. O., V. O. Vakhnenko, T. J. Shankland, and J. A. TenCate, 2006, Soft-ratchet modeling of slow dynamics in the nonlinear resonant response of sedimentary rocks: *Conference Proceedings, American Institute of Physics*, **838**, 120–123.
- Walsh, J. B., 1965, The effect of cracks on the compressibility of rock: *Journal of Geophysical Research*, **70**, 381–389, doi: [10.1029/JZ070i002p00381](https://doi.org/10.1029/JZ070i002p00381).
- Winkler, K. W., and X. Liu, 1996, Measurements of third-order elastic constants in rocks: *The Journal of the Acoustical Society of America*, **100**, 1392–1398, doi: [10.1121/1.415986](https://doi.org/10.1121/1.415986).
- Winkler, K. W., and L. McGowan, 2004, Nonlinear acoustoelastic constants of dry and saturated rocks: *Journal of Geophysical Research, Solid Earth*, **109**, 67–85, doi: [10.1029/2004JB003262](https://doi.org/10.1029/2004JB003262).
- Wu, T. T., 1966, The effect of inclusion shape on the elastic moduli of a two-phase material: *International Journal of Solids and Structures*, **2**, 1–8, doi: [10.1016/0020-7683\(66\)90002-3](https://doi.org/10.1016/0020-7683(66)90002-3).
- Zhang, J. J., and L. R. Bentley, 2003, Pore geometry and elastic moduli in sandstones: *CREWES Research Report*, **15**, 1.1–1.20.
- Zhang, L., J. Ba, L. Fu, J. M. Carcione, and C. Cao, 2019, Estimation of pore microstructure by using the static and dynamic moduli: *International Journal of Rock Mechanics and Mining Sciences*, **113**, 24–30, doi: [10.1016/j.ijmms.2018.11.005](https://doi.org/10.1016/j.ijmms.2018.11.005).
- Zimmerman, R. W., W. H. Somerton, and M. S. King, 1986, Compressibility of porous rocks: *Journal of Geophysical Research*, **91**, 12765–12777, doi: [10.1029/JB091iB12p12765](https://doi.org/10.1029/JB091iB12p12765).

Biographies and photographs of the authors are not available.